JACS
JOURNAL OF THE AMERICAN CHEMICAL SOCIETY

ARTICLE

pubs.acs.org/JACS

Supramolecular Aggregation of Block Copolymers in the Solid State As Assisted by the Selective Formation of Inclusion Crystals

Silvia Bracco, Angiolina Comotti,* Lisa Ferretti, and Piero Sozzani

Department of Materials Science, University of Milano Bicocca, Via R. Cozzi 53, 20125 Milano, Italy

Supporting Information

ABSTRACT: Supramolecular self-assembly of a host molecule with selected blocks of triblock copolymers enabled the formation of inclusion 2D nanocrystals that connect consecutive copolymer chains. Indeed, the selective inclusion of ethylene oxide (EO) blocks in inclusion crystals and the phase segregation of PO blocks of poly(ethylene oxide-*b*-propylene oxide-*b*-ethylene oxide) ($EO_nPO_mEO_n$) triblock copolymers provide an efficient route to create alternated crystalline lamellae and amorphous layers, forming a well-organized material. The spontaneous formation of the supramolecular architectures was realized by a solvent-free mechanochemical approach or by thermal treatment of the copolymer and host (tris-*o*-phenylenedioxycyclotriphosphazene), as demonstrated by in situ synchrotron X-ray diffraction. The driving force for the fabrication of crystalline inclusion compounds with selected EO segments is based on the establishment of cooperative noncovalent intermolecular interactions, while steric effects prevent the formation of the inclusion crystal with the remaining PO blocks. The 2D $^{1}H-^{13}C$ solid state and fast-^{1}H MAS NMR provide direct evidence of the intimate interactions between the host and EO block and the topology of the block copolymer in the material. The large magnetic susceptibility generated by the aromatic host nanochannels surrounding the included EO chains was interpreted by ab initio calculations (HF-GIAO/DGDZVP) that carefully reproduce the chemical shifts associated with the effects of guest−host interactions. The theoretical calculations enable the measurement of short intermolecular distances between the host and the target block, demonstrating the existence of a diffuse network of multiple CH$\cdots\pi$ host−guest interactions that improve the robustness of the supramolecular architecture. The overall evidence enforces the strategy of combining the use of block copolymers and clathrate-forming molecules to fabricate organized materials through noncovalent interactions.

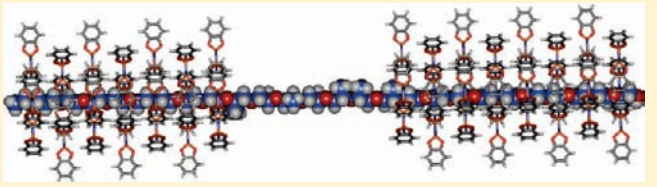

INTRODUCTION

Presently, much effort is being put into the preparation of well-defined supramolecular materials of precisely controlled structure and morphology, through the self-assembly of properly engineered molecules and macromolecules that enable the construction of diverse and complex architectures on molecular and nanometric hierarchical scales.[1] In this field, block copolymers play an important role as they provide a full range of interactions to govern assembly on the molecular scale, while phase segregation directs, most effectively, assembly on the nanoscale.[2] Chain segments endowed with amphipathic structures self-assemble into separate, but still connected, nanodomains, leading to a variety of aggregation motifs.[3] The phase segregation induced by the blocks' differential affinity to a solvent enabled the formation of supramolecular periodic structures and mesophases with increasing morphological complexity, such as gyroids, helices, nanotubes, and hollow spheres.[4] The application of copolymer mesophases as templating scaffolds for the condensation of metal oxides allowed the fabrication of mesoporous structures and nanoparticles of intriguing architectures, which are the mesophase replica.[5]

In the bulk, nanophase segregation leads to the copolymers spontaneously forming organized architectures endowed with distinct optical, mechanical, and morphological features.[6] Such organization in glassy, and crystalline domains of single polymeric blocks can determine an exquisite morphological sophistication and can ameliorate mechanical properties.[7] However, the resulting supramolecular structures are determined by the synthesis of a specific copolymer, and how the copolymer spontaneously aggregates, according to the nature of the single blocks. The fine-tuning of the aggregation is achieved by tailoring the copolymer-block arrangement, the relative chain length, the differential rigidity, and the chemical identity of the blocks.[8]

The perspective of a larger variety of morphologies and structures is reached if interplay with a second component imparts greater complexity. This was realized by several strategies that sometimes took inspiration from natural materials. Indeed, the use of synergistic interactions between nanoparticles and block copolymers based on a biomimetic approach has provided new opportunities for designing hierarchical structures and has led to the development of functional hybrid materials with tailored electrical, magnetic, and photonic properties.[9] The addition of a second "active" component, such as a low molecular mass compound, permits the exploration of

Received: February 18, 2011
Published: May 18, 2011

dx.doi.org/10.1021/ja201551n | *J. Am. Chem. Soc.* 2011, 133, 8982–8994

Scheme 1

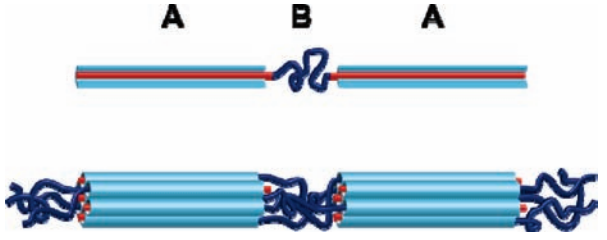

noncovalent interactions that guide the supramolecular aggregation of the copolymer, through molecular recognition of a selected block.[10] Similarly, the formation of pseudorotaxanes with block copolymers is based on selective recognition with a designated block.[11]

The concepts of supramolecular self-assembly by soft interactions can be applied to direct a copolymer's solid state organization by the selective incorporation of a single block into inclusion crystals. Our strategy encompasses the use of an "active" host molecule that easily crystallizes with target copolymer segments in the solid state to form nanocrystalline domains of inclusion compounds, realizing an unusual copolymer assembly that forms supramolecular buildings of orderly arranged nanocrystals. While the selected blocks are engaged by the inclusion crystal formation, the remaining blocks occupy the intercrystalline regions and behave as amorphous connectors between nanocrystalline domains. Such an inclusion-assisted assembly with copolymers can be utilized successfully to create materials with soft and hard layers regularly alternated within the molecular building. By using suitable ABA triblock copolymers, the two outer blocks (A) can be employed in the formation of inclusion crystals, while the inner block (B) can be segregated to form an amorphous phase (Scheme 1). The selected blocks (A) become the guest of the host−guest crystals, acting as a molecular adhesive and uniting the consecutive copolymer chains. The driving force that lies behind the fabrication of 3D supramolecular architectures is the tendency of the "active" molecules to self-assemble with selected copolymer blocks through specific noncovalent intermolecular interactions, while the steric effects prevent the formation of the inclusion crystal with the remaining blocks.

A few molecular hosts, such as cholic acids,[12] urea,[13] perhydrotriphenylene,[14] and tris-*o*-phenylenedioxycyclotriphosphazene (TPP),[15] have proved to be selective for the entrapment of elongated chains with limited steric encumbrance of the lateral substituents and represent good candidates for the selective enclatharation of specific homosequences of block copolymers in inclusion crystals. TPP molecules can form crystalline hexagonal structures endowed with parallel and independent channels that are ideally suited for the inclusion of macromolecules, and selectivity toward linear chains is provided not only by the channel cross section (about 5 Å) but also by aromatic groups that line the channel walls and form persistent supramolecular CH$\cdots\pi$ interactions with the guests.[16] A great advantage of TPP molecules is their easy self-assembly with linear molecules by thermal treatment, or by a few minutes of simple grinding, as recently demonstrated by the segmental enclathration of the polybutadiene homopolymer in the solid state.[17] Indeed, the TPP molecule offers the possibility of applying a solvent-free mechanochemical approach[18] to form supramolecular structures and fabricate nanomaterials. The mechanochemical approach is attractive for its implications in green technologies and, more recently, for promoting supramolecular aggregation.

Here, we have demonstrated that TPP molecules are able to recognize copolymer homosequences and selectively entrap ethylene oxide sequences in poly(ethylene oxide-*b*-propylene oxide-*b*-ethylene oxide) triblock copolymers of varied sequence lengths, resulting in the formation of distinct crystalline nanodomains connected one to another by the propylene oxide amorphous phase. For comparison, the inclusion behavior of random ethylene oxide−propylene oxide copolymers was addressed. The formation of the inclusion crystals could be realized by thermal treatment or by grinding a mixture of the two solid-state components. The formation of the binary adducts and the selective inclusion of copolymer chains was determined unequivocally by in situ powder X-ray diffraction with synchrotron radiation, solid-state NMR, calorimetric analysis, and ab initio calculations, while scanning electron microscopy revealed the morphological architecture. The newly formed compounds are highly stable and melt at temperatures much higher than the pure host and the copolymer. This notable behavior could be interpreted in terms of the establishment of noncovalent intermolecular interactions that drive the spontaneous assembly and cooperatively sustain the robust supramolecular architecture.

RESULTS AND DISCUSSION

Selective Encapsulation of Copolymer Blocks in Inclusion Crystals. The TPP/copolymer materials were prepared by mechanochemical grinding or by thermal treatment of a solid-state mixture of the copolymer and the TPP host. Pure TPP displays polymorphism forming close-packed and porous structures: the porous structure presents a hexagonal lattice and contains open nanochannels of about 5 Å cross section,[19] while the close-packed architecture exhibits a monoclinic structure with no cavities[20] (Supporting Information Figure S1). In the case of the close-packed monoclinic structure, there is a significant overall rearrangement that takes place during the formation of the adducts; instead, an isostructural transition occurs from the porous TPP to the inclusion crystal. The self-assembly between TTP crystals and poly(ethylene oxide-*co*-propylene oxide) copolymers (Figure 1) leads to the formation of high-melting adducts, which exhibit a congruent melting at temperatures as high as 573 K. The availability of different poly(ethylene oxide-*co*-propylene oxide) (EO−PO) copolymer microstructures spanning triblock copolymers of different molecular weights ($EO_mPO_nEO_m$) to random copolymers (Table 1) enables peculiar arrangements and selective confinement of the copolymer sequences in the TPP nanochannels.

The spontaneous adduct formation, by heating a mixture of TPP crystals in either their close-packed or porous structure form, and the copolymers was followed in situ by calorimetric analysis (Figure 2). The stoichiometric mixtures, typically TPP/copolymer ratio of 0.20, were prepared directly in a DSC crucible. In the case of the F108 block copolymer with the longest EO homosequences (Figure 2A), the DSC trace shows first the melting of the EO segments of the copolymer at 331 K, followed by the melting endotherm of TPP at 518 K.[15] The second phenomenon occurs simultaneously with the self-assembly

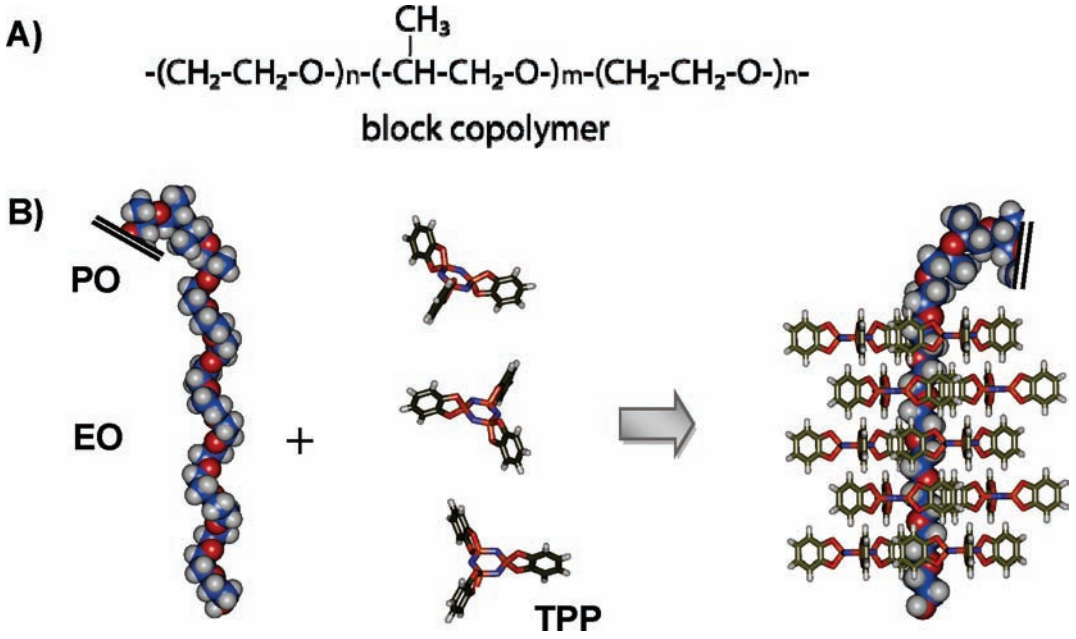

Figure 1. (A) Schematic representation of the poly(ethylene oxide−propylene oxide−ethylene oxide) triblock copolymer. (B) The ethylene oxide segment and TPP molecules (left) self-assemble, forming the inclusion crystal. A segment of the EO copolymer chain included in the nanochannel of the TPP host (right) is reported. The copolymer chain is represented with van der Waals radii, and the TPP molecules are shown using the stick representation. The distance between the polymer hydrogen atoms and the center of the host aromatic moieties is about 2.8 Å.

Table 1. Molecular and Physico-chemical Parameters of Poly(ethylene oxide-*co*-propylene oxide) Copolymers and Their Inclusion Crystals (ICs)

copolymer	composition	M_n (g mol^{-1})	M_w/M_n	PEO (mol %)[a]	T_m (K) copolymer	T_m (K) TPP IC
PE6800	$EO_{71}PO_{30}EO_{71}$	8000		80	325	559
Pluronic F68	$EO_{76}PO_{29}EO_{76}$	8400	1.1	84	327	573
Pluronic F127	$EO_{102}PO_{62}EO_{102}$	12 600	1.2	77	329	561
Pluronic F108	$EO_{132}PO_{52}EO_{132}$	14 600	1.2	86	331	573
ran-copolymer	EO/PO = 0.82/0.18	12 000		82	270	563

[a] Determined by ^{1}H NMR.

exotherm of the adduct (Figure 2A, highlighted red). The adduct melts at far higher temperature (573 K), and its melting peak was accompanied by the decomposition of the copolymer. Similar behavior was observed for the block copolymers with shorter EO homosequences (Supporting Information). Starting from a mixture of TPP and the random copolymer, the DSC trace shows, at temperatures lower than 298 K, typical transitions of a statistical copolymer that develops a low degree of crystallinity, that is, the glass transition at 205 K, a crystallization peak at 223 K, and a broad melting at 253−273 K (Figure 2C). After the melting of TPP at 518 K, the self-assembly exotherm for the formation of the adduct can be clearly observed. The adduct melts at 563 K, and the phenomenon overlaps the degradation exotherm of the copolymer. The crystalline TPP adducts showed congruent melting with higher temperatures (563−573 K) than the two constituents, demonstrating the exceptional stability of the crystalline adduct.

The mechanochemical treatment was proved to be a valuable and easy method to fabricate the adducts in quantitative amounts: the copolymer and TPP were mixed and ground in an agate mortar for 5−10 min without the use of any solvent. Simply grinding TPP in the close-packed crystal structure form with the copolymers at room temperature causes it to undergo mechanochemical changes, bringing about the formation of TPP/copolymer materials. Even though the molecular motion is restricted in the solid state, the TPP molecules were able to rearrange around the copolymer, leading to the formation of more stable supramolecular adducts. Figure 2B shows the calorimetric scan of the sample obtained after grinding where the endotherm peak of melting, at about 573 K, superimposes the exotherm peak of the copolymer degradation. No melting peak of the pure host at 518 K and no trace of the pure copolymers were detectable. A similar DSC trace was detected for the adducts prepared starting from the porous crystalline polymorph of the host, which contains empty nanochannels prone to accommodate the copolymer chains. The melting of the adducts is notably 50 K higher than the melting of pure host crystals and about 240 K higher than the pure copolymers, widening the existence range of the copolymer in the solid state. By comparison, the supramolecular adducts with both random and block copolymers of different molecular weights were also obtained by cocrystallization of the two components in *o*-xylene solution. The DSC traces of the adducts show the temperature melting at ca. 573 K,

dx.doi.org/10.1021/ja201551n |*J. Am. Chem. Soc.* 2011, 133, 8982–8994

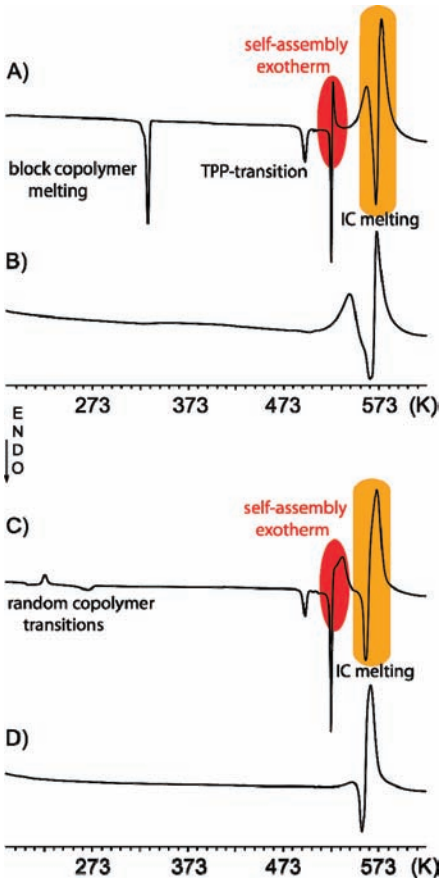

Figure 2. Differential scanning calorimetry runs from 183 to 623 K of (A) TPP and F108 and (C) TPP and *ran*-copolymer mixtures that show in situ formation of the TPP/copolymer adducts by thermal treatment. The self-assembly exotherm for the formation of the inclusion crystal is highlighted red, while the melting of the adduct is highlighted orange. Calorimetric scans of the (B) TPP/F108 and (D) TPP/*ran*-copolymer adducts as prepared in an agate mortar by grinding a mixture of the host and guest. The endotherm peak at 497 K corresponds to a solid−solid phase transition associated with pure TPP.[15] The weight fractions of the copolymer correspond to 0.2. The heating rate is 10 K/min.

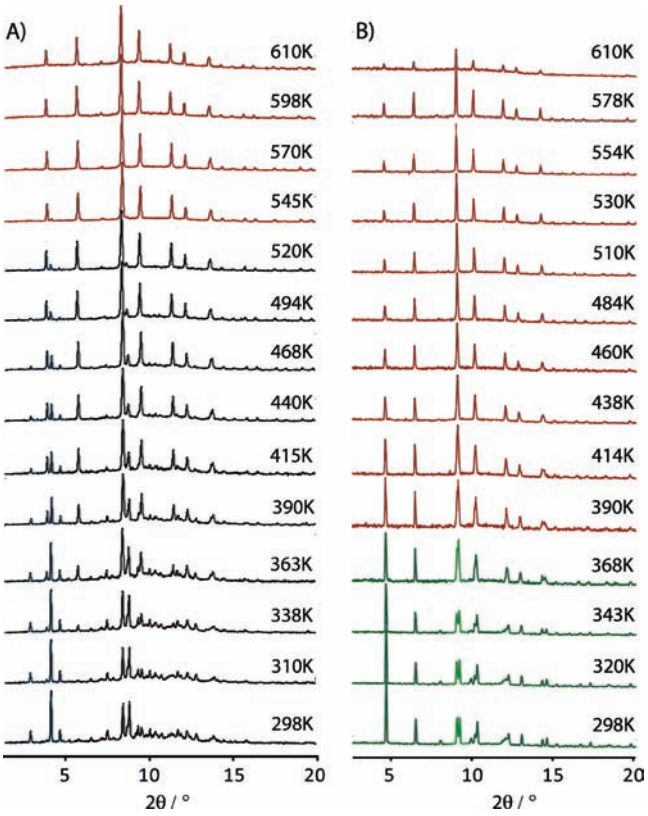

Figure 3. In situ synchrotron powder diffraction patterns of a powder mixture containing TPP and the F68 block copolymer as a function of temperature. The formation of the TPP/block copolymer adduct, which exhibits a hexagonal unit cell (red line), was followed, starting from two distinct guest-free TPP polymorphs: (A) close-packed TPP structure with a monoclinic unit cell (black lines) and (B) porous crystalline TPP structure with a hexagonal unit cell (green lines). The thermal expansion coefficients for the hexagonal unit-cell parameters of the adduct are $\alpha_a = \partial(\ln a/\partial T)_p = 1 \times 10^{-4}$ K^{-1} and $\alpha_c = \partial(\ln c/\partial T)_p = 5 \times 10^{-5}$ K^{-1}.

together with the degradation of the copolymer (Supporting Information).

The formation of the inclusion crystals and the phase changes were followed in situ by synchrotron X-ray diffraction of a mixture of TPP and the copolymer during heating treatment. Starting from guest-free TPP, the structural reorganization was followed as function of temperature. Synchrotron radiation, given its high energy beam and intense response, allowed us to efficiently follow the evolution in situ of the structures. Consequently, mechanistic information of structural changes and phase transformation during adduct formation was highlighted. For the synthesis of the TPP/F68 adduct, a crystalline powder of TPP was mixed with the F68 block copolymer and put into a quartz capillary tube, which was heated with a scanning rate of 1 K/min. Figure 3 shows in situ XRD patterns. At room temperature, the XRD pattern of the mixture prior to heating (black line) is consistent with the close-packed monoclinic TPP structure (space group $P2_1/n$, a = 25.4193(9) Å, b = 5.9125(13) Å, c = 25.591(9) Å, β = 95.944(20), V = 3825.4(13) Å^3)[20] together with a few diffraction peaks associated with the block copolymer crystalline phase. Plotting individual patterns at the different temperatures illustrates details of the formation of the adduct. Heating the powder mixture results in the reduction reflections of the monoclinic phase and new peaks appear, which are assigned to the crystalline phase of the inclusion crystal. In particular, the characteristic diffraction peak for the monoclinic phase at 2θ = 4.83° decreases progressively and the peak at 2θ = 4.57° increases. The powder pattern of the new phase is consistent with the formation of a hexagonal structure. At the melting temperature of the host matrix (518 K), the transformation of the close-packed monoclinic phase to the new phase of the adduct goes to completion. Further thermal treatment at higher temperatures shows that the crystalline structure of the adduct can exist up to about 600 K. All of the diffractograms in the 310−545 K range were refined by the Rietveld method considering two phases, the monoclinic phase of pure TTP and the hexagonal structure of the adduct. The crystalline structure of the TPP/F68 adduct at 545 K was refined with the hexagonal space group $P6_3/m$, a = 11.6577(6) Å, c = 10.172(10) Å, and V = 1197.16(14) Å^3 (for TPP/F108 adduct at 545 K: space group $P6_3/m$, a = 11.6764(6) Å, c = 10.1888(10) Å, and V = 1203.01(14) Å^3). The crystal structure of the TPP/copolymer adducts exhibits a hexagonal lattice, forming nanochannels of about 5 Å cross section built by the paddle-wheel shaped

molecules of TPP that line the walls with the phenylenedioxy aromatic units and face the channels. The difference Fourier map revealed the presence of electron density along the *c*-axis distributed in the center of the channels, suggesting the encasing of at least a block of chains inside the channels.

The adduct could also be prepared starting from the porous TPP structure that presents empty nanochannels prone to include the copolymer guests[19] (Figure 3B). The XRD pattern of the mixture prior to heating is consistent with the hexagonal unit cell of empty-pore TPP (space group $P6_3/m$, a = 11.4125(6) Å, c = 10.1193(8) Å, V = 1141.41(11)), and no residual electron density is observed in the nanochannels. On heating the mixture of porous TPP and the F68 block copolymer, there occurs an isostructural transition from the porous TPP to the adduct, and a discrete change of the unit-cell parameters appears at about 363 K (Figure 4).[21] In particular, the *a*- and *b*-axes expand and the *c*-axis contracts, while the unit-cell volume shows a sudden increase. Further heating to 573 K causes the *a*- and *b*-axes to enlarge and the *c*-axis to reduce continuously, and the unit-cell volume shows, concomitantly, a gradual increase over the entire range (all of the powder patterns fit in the hexagonal space group $P6_3/m$). The discrete increase of the unit-cell parameters at 363 K indicates the adduct formation, which occurs after the melting of the EO block of the copolymer. Actually, at high temperature the Fourier difference maps show the presence of electron density along the channel.

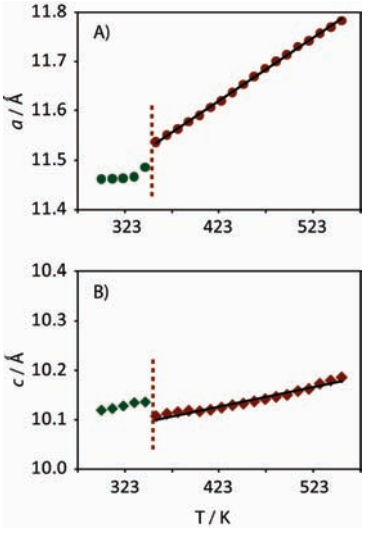

Figure 4. Temperature evolution of structural parameters for the formation of TPP/F68 block copolymer starting from a mixture of TPP hexagonal structure and block copolymer: (A) lattice constant a = b; (B) lattice constant c. The green markers refer to the lattice constants of the TPP hexagonal unit cell; the red markers are the lattice constants of the adduct. The black lines represent the linear fitting of the unit-cell parameters versus temperature for the TPP/block copolymer: the unit-cell parameters a and c expand with a rate of $(\partial a/\partial T)_p = 1.3 \times 10^{-3}$ Å K^{-1} and $(\partial c/\partial T)_p = 4 \times 10^{-4}$ Å K^{-1}. The thermal expansion coefficients for the hexagonal unit-cell parameters are $\alpha_a = (\partial \ln a/\partial T)_p = 1 \times 10^{-4}$ K^{-1} and $\alpha_c = (\partial \ln c/\partial T)_p = 5 \times 10^{-5}$ K^{-1}.

Moreover, the formation of the inclusion crystals with *ran*-copolymer was also followed in situ by collecting X-ray diffraction patterns as a function of temperature of a mixture of the two molecular components, TPP and the random copolymer (Figure S9). In this case, the random copolymer is liquid at room temperature, and its addition to the monoclinic TPP crystals results in the immediate formation of a substantial amount of the adduct. On raising the temperature, the content of the adduct gradually increases, and transformation is accomplished at the melting of pure TPP, which occurs at 518 K. The XRD powder patterns at higher temperatures demonstrate that also the adduct with the random copolymer persists up to about 600 K, while in the powder pattern at 613 K a lower S/N ratio is visible because of its partial melting. The adduct with the random copolymer was prepared also starting from porous TPP. Interestingly, the addition of the random copolymer to the porous TPP led, already at room temperature, to a complete formation of the adduct (not shown). In the XRD powder pattern, no peaks of the porous TPP crystal phase were observed (i.e., no splitting of the peak at 2θ = 8−9°); instead, the powder profile presents, already at room temperature, peaks ascribed to the inclusion crystals ($P6_3/m$, a = 11.5317(4) Å, c = 10.0750(6) Å, V = 1160.27(8) Å^3) and a strong decrease of the (001) peak intensity because of the reduced electron density contrast between the walls and the cavity due to the channel filling with the copolymer.

During the formation of the supramolecular architectures of the binary adducts, the TPP crystalline structure arranges to accommodate the polymer chains and minimize the lattice energy. The effect of the chain confinement on the crystal structures can be observed comparing the lattice parameters of the XRD patterns collected at room temperature (Table 2). The cell parameters a (and b) enlarge from 11.4353(4) Å in the empty TPP to 11.5153(4) Å in the adduct with F68 and up to 11.5497(5) Å in the TPP/random copolymer. Consequently, the cross section of the channels of the adduct with the random copolymer became greater than that of the adducts with block copolymers. The a (and b) unit-cell parameters and the channel cross section of the TPP/block copolymers (F68 and F108) are close to those of the TPP/PEO adduct ($P6_3/m$, a = b = 11.4830(4) Å, and c = 10.0481(8) Å), suggesting that the ethylene oxide sequences in the channels of about 5 Å are selectively included. Contrarily, the larger nanochannel cross section in the TPP/random copolymer indicates that also the

Table 2. Unit-Cell Parameters and Volume of the TPP Inclusion Crystals[a]

compound	space group	a,b (Å)	c (Å)	V_{cell}[b] (Å^3)	V_{void}[c] (Å^3)	V_{void}/V_{cell}
TPP/random cop.	$P6_3/m$	11.5497(5)	10.0148(7)	1156.95(6)	377.96	0.327
TPP/F68	$P6_3/m$	11.5153(4)	10.0814(6)	1157.72(8)	352.51	0.304
TPP/F108	$P6_3/m$	11.4939(3)	10.0694(6)	1152.05(8)	342.59	0.297
TPP	$P6_3/m$	11.4353(4)	10.1420(5)	1148.55(7)	344.73	0.300

[a] The crystal structures were refined using the Rietveld method. [b] V_{cell} values are unit-cell volumes obtained from crystallographic data. [c] Molecular volume calculations were performed using the Accelrys Materials Studio v.4.2 modeling suite. The volumes of channels V_{void} were determined with a Connolly surface using probe radius of 0.5 Å and an ultrafine grid spacing, after removal of guests.

dx.doi.org/10.1021/ja201551n |*J. Am. Chem. Soc.* 2011, 133, 8982–8994

bulkier propylene oxide monomer units are confined inside the channels.

The host framework is based on a network of weak interactions among the paddle-wheel-shaped phenylenedioxy moieties that protrude outside the central phosphazenic ring in a high symmetry fashion. As a consequence of the soft network of weak interactions, the host architecture can adjust to satisfy the steric requirements of the guests and tolerate channel expansion (Figure 5). The transformation is assisted by the establishment of intermolecular host−guest interactions that guide the self-assembly of the polymer chains in the nanochannels and the formation of the stable adducts. Notably, the included polymer chains can assume multiple conformations, and the systems appear not to be commensurate.

Host−Guest Relationships of Specific Copolymer Blocks in the Nanophases. A precise determination of intermolecular host−guest interactions is of great importance for molecular recognition and structural characterization, especially in the presence of disordered guests. The ability of TPP channels to induce the selective inclusion of alkylene oxide monomer units of copolymers with different microstructures, from statistical to block distribution, was unambiguously demonstrated by solid-state NMR. Solid-state NMR is a powerful tool for the structural and dynamical characterization of supramolecular systems, and the identification of the local environment in which guest molecules reside.[22] The detection of small differences in the chemical surroundings of the nuclei enables the extraction of structural information as well as guest location and dynamics. Moreover, multinuclear solid-state NMR permits the deduction of key intermolecular distances: 2D heteronuclear experiments correlating ^{1}H and ^{13}C resonances can provide the constraints for structural determination.[23] Notably, the structures of organic crystals containing aromatic moieties can be described in-depth by NMR spectroscopy as ring currents can produce magnetic susceptibility effects[24] that provide a direct evidence of the selective inclusion of copolymer chain segments.

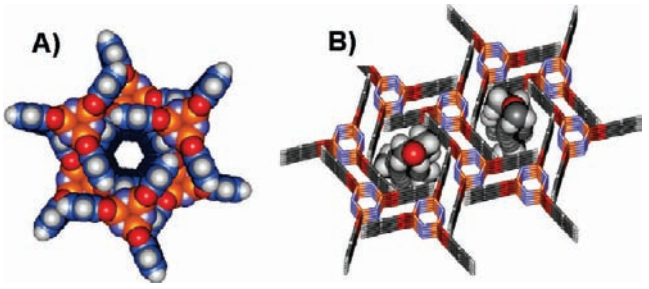

Figure 5. (A) The hexagonal crystal structure presents a one-dimensional channel made by paddle-wheel shaped TPP molecules that line the walls with their phenylenedioxy aromatic units facing the channels. (B) The complementary shapes of the TPP nanochannels and the poly(ethylene oxide) chains facilitate association through supramolecular interactions.

^{13}C MAS NMR spectra of both the adducts and the pure copolymers are reported in Figure 6. The chemical shift changes of the copolymers in the TPP architecture with respect to those in the bulk reflect the distinct chemical environments that the copolymers experience. The spectra of TPP/copolymer can be interpreted following the assignment of the NMR spectra of the pure copolymers. The dyads of the monomer units ethylene oxide [E] and propylene oxide [P] are here denoted using square brackets. The ^{13}C CP MAS NMR spectrum of the TPP/block copolymer (Figure 6A) presents, in addition to the aromatic TTP signals (not shown), a few aliphatic signals of the copolymer chains in the 10−80 ppm range. The signals of the copolymer appear far different in the spectra of the adduct as compared to those of the bulk (Figure 6B), both from the point of view of chemical shift and spectral response, because the polymer blocks participate in distinct phases of quite a different nature (i.e., crystalline/amorphous or included/bulk phases). The TPP/block copolymer spectrum exhibits a major signal at δ_C = 68.4 ppm that is due to the ethylene oxide homosequences [EE] and shows a considerable upfield shift with respect to the corresponding signals in the bulk (Figure 6A, highlighted blue). Indeed, the [EE] homosequences of the pure copolymer present two peaks, at δ_C = 71.2 and 72.5 ppm: the narrow peak corresponds to the amorphous phase $[EE]_{am}$, while the broader peak is due to the crystalline phase $[EE]_{cry}$.[25] Upon confinement

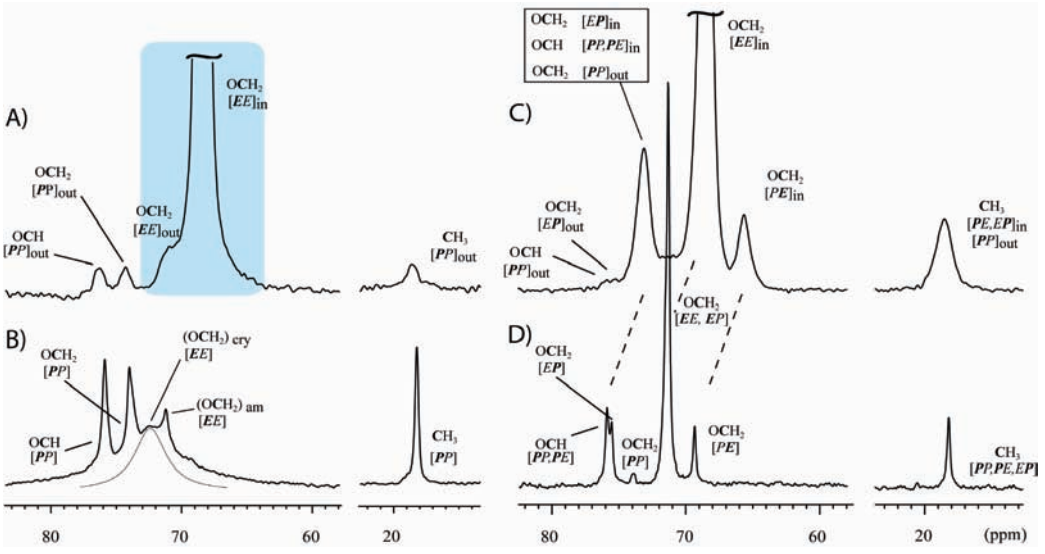

Figure 6. (A) ^{13}C CP MAS of TPP/F108 adduct and (B) ^{13}C MAS of the pure block copolymer F108. (C) ^{13}C CP MAS of TPP/random copolymer adduct and (D) ^{13}C MAS of the pure random copolymer.

dx.doi.org/10.1021/ja201551n |J. Am. Chem. Soc. 2011, 133, 8982–8994

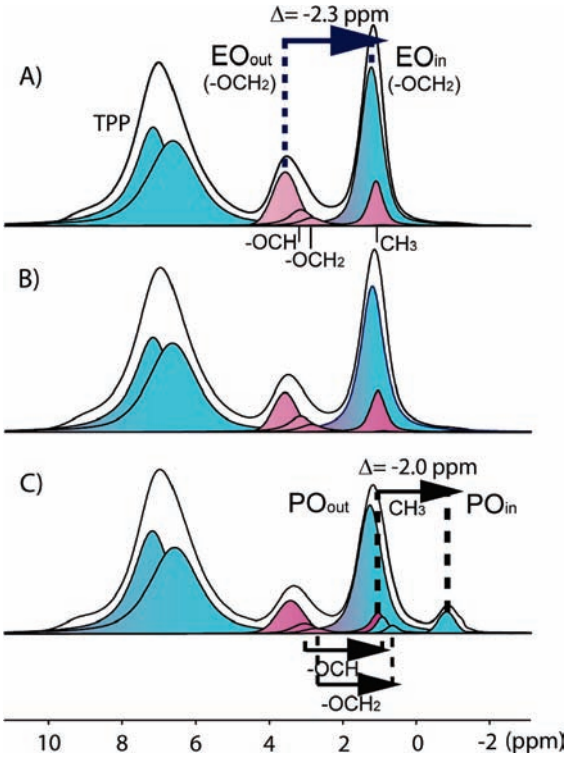

Figure 7. 500 MHz fast-^{1}H MAS (35 kHz) NMR spectra of (A) TPP/F108, (B) TPP/F68, and (C) TPP/random copolymer materials. The signals of the copolymer moieties confined in the nanochannels of the inclusion crystals are indicated as EO_{in} and PO_{in}, while those of nonincluded copolymer moieties are indicated as EO_{out} and PO_{out}. The signals of both TPP and the copolymer moieties that belong to the inclusion crystalline nanophases are highlighted blue. Segments of copolymers in the amorphous nanophases are highlighted violet.

in the TPP architecture, the [EE] sequences exhibit a large upfield shift of $\Delta\delta_C = -2.8$ ppm with respect to the signal in the amorphous phase of the pure copolymer and, even more impressively, of $\Delta\delta_C = -4.1$ ppm as compared to the signal of the poly(ethylene oxide) crystalline phase (Table 3). The remarkable upfield shift arises mainly from the magnetic susceptibility generated by the aromatic rings of the host facing the ethylene oxide homosequences $[EE]_{in}$ in the nanostructured material, as discussed later, and clearly demonstrates the inclusion of the homopolymer sequences in the TPP nanochannels. A further contribution to the upfield shift is ascribed to the conformational arrangement of the ethylene oxide homosequences that differ from that of the bulk. In the nanochannels, although the molecules are squeezed to elongated shapes, departure from trans conformations is tolerated, and γ-gauche shielding effects contribute with the same sign to the magnetic susceptibility.[26] The shoulder at $\delta_C = 70.9$ ppm in the TPP/copolymer spectrum indicates the presence of a small amount of [EE] units, $[EE]_{out}$, that reside outside the TPP matrix. On the contrary, the resonances of the OCH, OCH_2, and methyl groups at $\delta_C = 75.9$, 74.0, and 18.6 ppm, respectively, that correspond to the propylene oxide homosequences [PP], do not present any relevant shift with respect to the pure block copolymer, revealing that the bulkier propylene oxide monomer units are excluded from the nanochannels. These results clearly demonstrate the selective confinement of the poly(ethylene oxide) blocks, the poly(propylene oxide) sequences being prevented from entering the channels and residing in the amorphous phase among the crystallites.

Table 3. ^{13}C SSNMR Chemical Shift (δ/ppm) of TPP/F68 ICs and TPP/F108 and Their Pure Block Copolymers

compound	observed mon. unit	chemical groups	dyad	δ (ppm) F68	δ (ppm) F108
TPP/copolymer	PO	OCH	$[\vec{P}\vec{P}]_{out}$	76.1	75.9
	PO	OCH_2	$[\vec{P}\vec{P}]_{out}$	74.3	74.0
	EO	$(OCH_2)_n$	$[EE]_{out}$	71.2	70.9
	EO	$(OCH_2)_n$	$[EE]_{in}$	68.4	68.4
	EO	OCH_2	$[\vec{P}E]$	69.2	
	PO	CH_3	$[\vec{P}\vec{P}]_{out}$	18.6	18.6
pure copolymer	PO	OCH	$[\vec{P}\vec{P}]$	75.8	75.9
	PO	OCH_2	$[\vec{P}\vec{P}]$	73.9	74.0
	EO	$(OCH_2)_{cry}$	$[EE]_{cry}$	72.4	72.5
	EO	$(OCH_2)_{am}$	$[EE]_{am}$	71.2	71.2
	PO	CH_3	$[\vec{P}\vec{P}]$	18.2	18.2

The ^{13}C CP MAS spectrum of the TPP sample with the *ran*-copolymer (Figure 6C) displays, in the 65−77 ppm range, three main resonances at $\delta_C = 65.6$, 68.5, and 73.1 ppm that are shifted upfield of at least $\Delta\delta_C = -2.8$ ppm as compared to the corresponding signals of the pure random copolymer (Figure 6D and Table S2). The intense signal at $\delta_C = 68.5$ ppm corresponds to the [EE] homosequences ($p_{EE} = 0.64$), while the two remaining resonances are mainly associated with the EO−PO heterosequences (OCH_2 in [PE] and [EP] and OCH in [PE] dyads). In this case, the propylene oxide monomer units are randomly distributed along the polymer chain, and the heterosequences have a much higher probability ($p_{EP,PE} = 0.32$) than those in the block copolymers where junctions between blocks are rare ($p_{EP,PE} = 0.02$). Consequently, also heterosequences are detectable in both the pure *ran*-copolymer and the adduct with TPP. The notable upfield shift of signals containing heterosequences clearly reveals that not only are the poly(ethylene oxide) sequences confined inside the channels, but also the propylene oxide monomer units in heterodyads are affected by the aromatic ring currents. Indeed, the ^{13}C signals at about $\delta_C = 75.9$ ppm of OCH of the propylene oxide unit move significantly upfield by $\Delta\delta_C = -2.8$ ppm, demonstrating that the propylene oxide units in proximity to the ethylene oxide units $[PE]_{in}$ are included inside the channels. The methyl resonance is not substantially shifted as compared to the bulk copolymer, suggesting that there are two contrasting effects: the magnetic subsceptibility shift added with the opposite sign to conformational effects.

High-resolution ^{1}H (500 MHz) MAS NMR spectra at rotation frequencies of 35 kHz reveal important features of the selective inclusion of copolymers in the aromatic nanochannels and provide a complementary perspective to the ^{13}C NMR spectra. The ^{1}H MAS NMR spectra of the pure block copolymers (not shown) exhibit two signals of equal intensity at $\delta_H = 1.1$ ppm and 3.6 ppm that are associated with the PO methyl and the remaining PO and EO hydrogens, respectively. The spectra of TPP/block copolymers exhibit two main signals of the copolymers, in addition to the TPP aromatic hydrogens at $\delta_H = 7.2$ and 6.7 ppm (Figure 7A and B and Table S3). The intensity ratio between the two copolymer signals becomes unbalanced in favor of the upfield

Table 4. Molar Fraction of EO with Respect to EO+PO, Molar Ratio of EO and PO Units inside the Channels, and Molar Fraction of the EO_{in} with Respect to the Host As Determined from the Analysis of the ^1H Peak Areas

	EO/(EO+PO) molar fraction	EO_{in}/EO_{tot} molar fraction	PO_{in}/PO_{out} molar ratio	EO_{in}/TPP molar ratio
TPP/F108	0.86	0.74	0	1.4
TPP/F68	0.83	0.82	0	1.4
TPP/ random	0.81	0.80	0.46	1.0

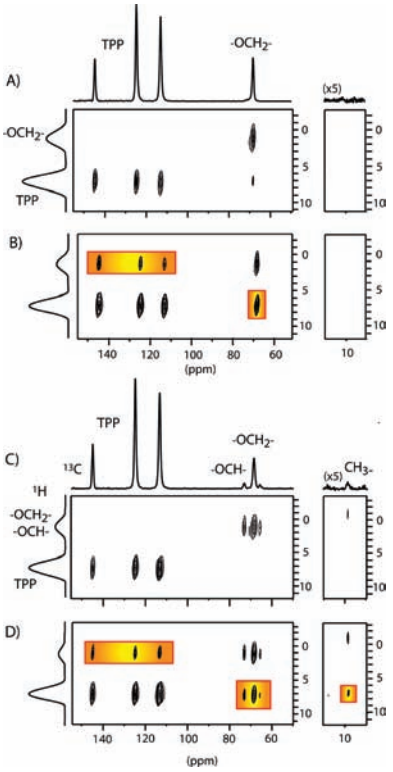

Figure 8. 2D $^1H-^{13}C$ PMLG HETCOR NMR spectra of TPP/random copolymer at two different contact times of 500 μs (A) and of 2.5 ms (B). 2D $^1H-^{13}C$ PMLG HETCOR NMR spectra of TPP/108 adducts collected at 500 μs (C) and 2.5 ms (D), respectively. The intermolecular interactions between the host and the copolymer are highlighted orange.

signal at δ_H = 1.1 ppm. This is due to the EO resonance that shifts upfield, from δ_H = 3.6 to 1.2 ppm, due to the magnetic susceptibility of the aromatic nanochannels. The absence of any other signal at higher fields clearly indicates that the PO methyl signal does not undergo any significant upfield shift, and only the EO sequences are selectively included in the channels, in agreement with ^{13}C NMR and XRD data. On the contrary, the random copolymer exhibits a notable upfield shift for the protons of the methyl in the TPP/*ran*-copolymer sample. The methyl hydrogens of PO units resonate at negative chemical shift $\delta_H = -0.9$ ppm - (CH_3 in PO_{in}) with an upfield shift of $\Delta\delta_H = -2.0$ ppm as compared to methyls in the bulk copolymer (CH_3 in PO_{out}). The exceptional upfield shift is explained by the large magnetic susceptibility effect of the aromatic matrix, unequivocally showing that methyl groups of PO units are confined inside the channels.

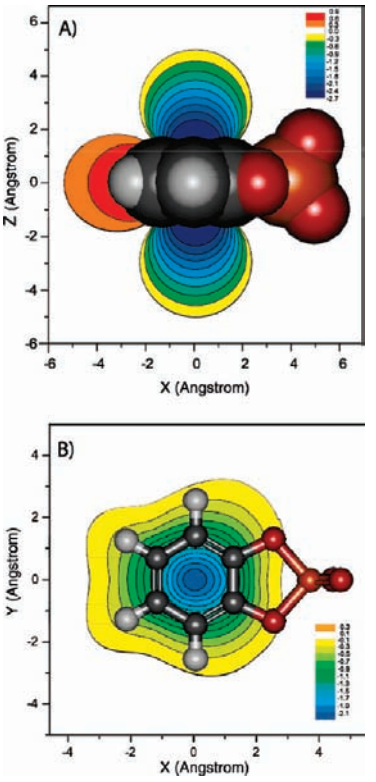

Figure 9. (A) Computed isoshielding surfaces perpendicular to the phenyledioxyphosphate plane (lateral view). (B) Shielding increment surfaces of the phenyledioxyphosphate molecule (top view) computed at 2.85 Å height above the aromatic plane. The color code reflects the chemical-shift change $\Delta\delta$ of the methane hydrogen placed at a particular position relative to the aromatic ring, as compared to the chemical shift of isolated molecule. The phenylenedioxyphosphate molecule is represented with van der Waals radii (above) and ball-and-stick (below).

For all of the adducts, the EO/EO+PO fraction corresponds to the value obtained in solution, indicating that the ^1H MAS spectra are the response of the whole copolymer (Table 4). The quantitative analysis of the ^1H NMR spectrum could give, independently, the amount of the PO confined inside the channels: a PO_{in}/PO_{out} molar ratio of 0.46 is determined when PO is randomly distributed along the polymer chains, as compared to the virtually absence of PO_{in} signal in the TPP/block copolymer adducts. The quantification of the amount of EO within the channels as compared to that out, an EO_{in}/EO_{tot} fraction of 0.8, led to the conclusion that the major part of EO is included, while a minor fraction participates in the interfacial region. In TPP/block copolymers, the crystalline adducts present the same molar ratio of 1.4 between the monomer unit of the included EO block and the TPP molecule. This value represents the number of EO monomer units occupying a channel segment equal to $c/2$ (5.04 Å) and enables the calculation of the monomer unit length of 3.5 Å as arranged in the nanochannels. This value is close to that proposed for the poly(ethylene oxide) in channel-like inclusion compounds with about 5 Å cross section wherein the chain adopts trans conformations for the C−C bond and explores gauche conformations about the C−O bonds.[27] Collectively, the above results proved that fast-^1H MAS NMR represents a unique method to quantify the amount of chain segments that are distributed among the nanophases and to describe the arrangement of the chains in the distinct environments.

dx.doi.org/10.1021/ja201551n |*J. Am. Chem. Soc.* 2011, 133, 8982–8994

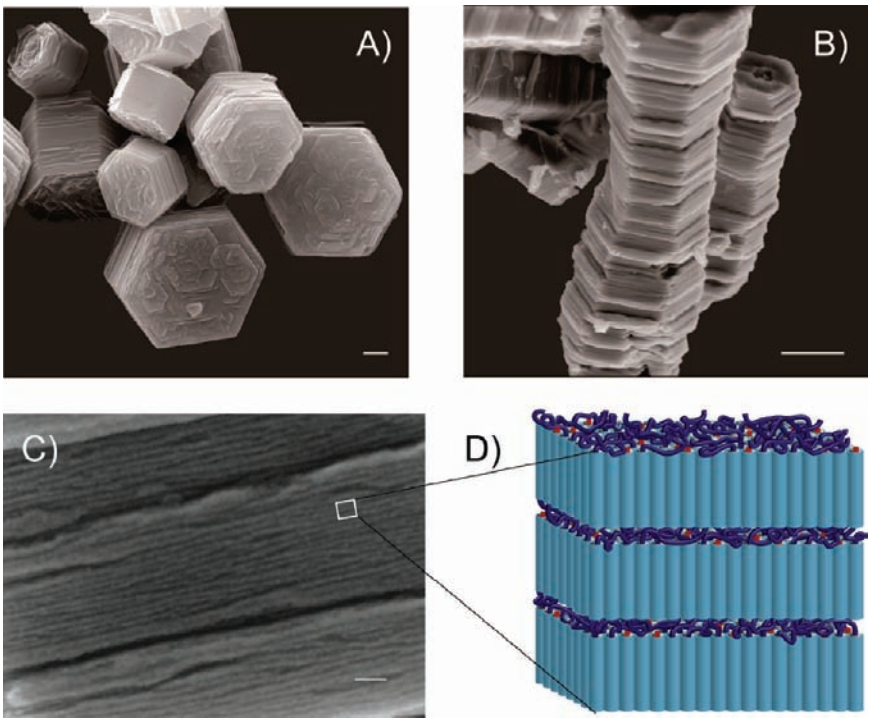

Figure 10. High-resolution scanning electron microscopy images of $EO_{132}PO_{52}EO_{132}$ triblock copolymer assembled with TPP in a supramolecular adduct: (A) hexagonal morphology of the crystals as viewed along the crystallographic *c*-axis ((001) face); (B) stacked hexagonal crystals as viewed perpendicular to the *c*-axis ((110) face). The reference bar is 2 μm. (C) Magnification of a lateral (110) face of the crystals showing the lamellar nanostructure with a repeat period of about 38 nm. The reference bar is 200 nm. (D) Schematic representation of the regularly alternated crystal and amorphous layers along the *c*-axis.

2D $^{1}H-^{13}C$ NMR spectra enable the detection not only of the distinct microenvironment explored by copolymer chains but also their respective host−guest relationships (Figure 8). Advanced 2D NMR spectroscopy experiments based on fast magic-angle spinning and phase modulated Lee−Goldburg decoupling (PMLG) reduce hydrogen−hydrogen homonuclear coupling, resulting in high resolution in the hydrogen domain.[28] Additionally, cross-polarization time rules the communication between the specific spins, that is, hydrogen and carbon, in the 2D experiment, and the cross peak intensities measure the distances according to the scaling law of $1/d_6$. Analysis of the TPP/block copolymer sample at a short contact time of 0.5 ms results in intramolecular host and guest correlations that are due to the polarization transfer to carbons from covalently bonded protons at less than 1.5 Å.[29] The signal of OCH_2 group of $[EE]_{in}$ is clearly observed, while no resonances of the propylene oxide homosequences appear because the PO segments reside outside the channels and consist of a highly mobile amorphous phase (above T_g) that prevents detection by $^{1}H-^{13}C$ cross-polarization experiments. Longer cross-polarization times (τ_c = 2.5 ms), which make cross-polarization effective at longer distances, result in new correlation signals (Figure 8B) that pertain to through-space intermolecular interactions between TPP and ethylene oxide nuclei, thus indicating an intimate relationship among the assembled components. The intense cross-peaks between the aromatic host moieties and the ethylene oxide sequences provide evidence of strong and frequent intermolecular magnetic interactions, demonstrating the selective confinement of the EO homosequences in the TPP nanochannels, while the PO units reside in the intercrystalline phase.

The 2D $^{1}H-^{13}C$ HETCOR NMR spectra of TPP/random copolymer sample clearly reveal the inclusion of both the EO homosequences and the mixed heterosequences in the TPP nanochannels. The inclusion of the propylene oxide sequences is apparent not only for the OCH and OCH_2 groups but also for the methyl group. At a short contact time (0.5 ms), the signals associated with intramolecular correlations were apparent in both the carbon and the hydrogen domains (Figure 8C). Unlike block copolymers, the [EP] and [PE] heterosequences cross polarize efficiently, being confined in the crystalline matrix. At longer contact times (2.5 ms), the aromatic hydrogens of the host correlate with the OCH, OCH_2, and even CH_3 carbons of the copolymer and vice versa (highlighted orange in Figure 8D).

High-resolution ^{1}H (500 MHz) MAS NMR combined with 2D HETCOR experiments provide access to structural information and key elements of supramolecular organization, intermolecular interactions, in host−guest adducts. The upfield shifts of the copolymers embedded in aromatic nanochannels are a clear demonstration of the intimate relationship of the guest with the host aromatic groups. The strong magnetic susceptibility, generated by the TPP aromatic moieties, permits the determination of the distance of the copolymer chemical entities relative to the phenylenedioxy rings. In particular, the ^{1}H chemical shifts of the copolymers in the adducts could be assigned to their site-specific arrangement with respect to phenylenedioxy moieties of the TPP host by quantum-chemical calculations. NMR chemical shifts were calculated using the gauge including atomic orbitals (GIAO) at the Hartree−Fock (HF) level with a DGDZVP basis.[30] Quantum-chemical calculations enable the determination of the through-space shielding effect generated by an

aromatic moiety on a probe molecule, that is, methane, and relate the chemical shifts displacements to the local structural features. Methane and phenylenedioxyphosphate were chosen as representative molecules to mimic the copolymer chemical units and the phenylenedioxy moieties of the TPP architecture, respectively. A methane molecule was placed at 240 specific positions with a distance ranging from 2.5−5.5 Å about the phenylenedioxyphosphate. The geometries of the phenylenedioxyphosphate and the probe molecule were optimized at the B3LYP/6-311G(d,p) level. HF-GIAO calculations of the NMR isotropic shielding value of the methane hydrogen in the distinct geometries mapped the through-space shielding effects (Figure 9A). The shielding shift ($\Delta\sigma$) at a given point was determined as the difference between the calculated isotropic shielding value of the proximal hydrogen of the probe molecule at that point relative to the phenylenedioxy ring and that of the hydrogen in the isolated methane. Figure 9 shows the resulting maps of the calculated proton NMR chemical shifts of methane relative to the isolated molecule $\Delta\delta$ (the chemical shift changes are equal in magnitude but opposite in sign to the shielding increments $\Delta\delta = -\Delta\sigma$).[31]

The aromatic ring generates the highest through-space magnetic shielding effect above and below the planar ring, while a weaker and reverse effect is observed beside the ring. Thus, the contour map enables an accurate determination of the distance of the guest hydrogens from the TPP aromatic rings when the shielding shift is known. In particular, the experimental shielding shift $\Delta\delta_H = -2.3$ ppm of methyl and methylene oxide hydrogens of the copolymer (as determined from the ^{1}H MAS NMR spectra) suggests that the copolymer hydrogens in the adducts are at a distance of 2.8−2.9 Å above the center of the molecular plane. Additionally, the shielding surface (reported as $\Delta\delta$) in the *XY* plane and at a distance of 2.85 Å above the aromatic plane reinforces the picture that the guest hydrogens lie above the center of the aromatic ring (Figure 9B). Short intermolecular distances, such as those here determined, imply close contact between the π-electron clouds and hydrogen atoms and favorable van der Waals interactions. The spatial arrangement is compatible with the occurrence of favorable CH···π interactions, as confirmed both by theoretical studies and by the survey of a number of crystal structure determinations, which have established that energy minima occur at distances of about 2.8 Å.[32]

The XRD structural resolution, although unable to detect the exact location of the guests, describes the crystal voids in which the guest moieties are encapsulated. The existence of CH···π interactions is compatible with the size of the 5 Å nanochannels in the crystal structure. Three contiguous phenylenedioxy rings are present at each cross section of TPP structure (Figure 5), and another three, related by a 6_3 screw axis, are found on the next TPP layer along the channel. Thus, all of the OCH_2, OCH, and CH_3 groups in the nanochannels find, with high probability, any of the π-receptors lining the walls and move to vicinal receptors through low activation energies. Multiple CH···π interactions simultaneously sustain the architecture and make a notable contribution to the exothermic self-assembly as detected by calorimetric analysis. Additionally, the diffuse network of CH···π interactions in the new adducts, through cooperation, contributes to the robustness of the supramolecular architectures that melt at temperatures higher than 573 K.

Nanoscale Organization of Inclusion Crystals. The partitioning of the copolymer blocks in phase-separated domains of the inclusion crystals and amorphous phase, established so far, can be expected to influence crystal morphology and architecture on higher hierarchical scales. High-resolution scanning electron microscopy images of the adducts could highlight the ordering on nano- and microscales. In Figure 10A, the morphology of the crystals clearly indicates a hexagonal-shaped contour that is compatible with the hexagonal $P6_3/m$ space group and suggests that we are observing the inclusion crystals along the *c* crystallographic axis ((001) face). The view perpendicular to the *c*-axis of the crystals ((110) faces) reveals the presence of columns of stacked prisms with hexagonal base (Figure 10B). Further magnification of the lateral faces of the prisms evidences a fine layered structure that consists of orderly arranged nanometric domains, which pack into a lamellar-like sequence (Figure 10C). The repeat period of about 38 nm parallel to the *c*-axis agrees with the regular alternation of crystalline and amorphous layers, in which the poly(ethylene oxide) homosequences are mainly included in the hexagonal inclusion crystals, while the poly(propylene oxide) units form the amorphous phase. Indeed, in the TPP/F108 adduct the elongated EO_{in} blocks align along the channel axis in the crystalline domains and occupy an overall height of 35 nm, while the PO blocks and interfacial EO_{out} segments participate in the amorphous phase that accounts for 3−4 nm.[33] The reason for the large height imbalance between the crystalline and amorphous domains becomes immediately evident when one considers that the copolymer chains can assume the quasi stretched conformation in the crystalline nanochannels and a coiled conformation in the amorphous phase. On the basis of these findings, we propose a model in which the end blocks of the triblock copolymer are locked into the channel-like inclusion crystals and the copolymer molecules are enchained, creating a new material of assembled nanocrystals regularly superimposed on one another.

CONCLUSION

The selective coupling of a molecular host with single blocks of $EO_nPO_mEO_n$ triblock copolymers has led to the fabrication of organized superstructures, which consist of crystalline domains connected by amorphous phases in an orderly fashion. Indeed, the arrangement of supramolecular crystalline nanodomains, in which the end EO blocks are anchored through multiple noncovalent interactions, is well controlled by the constraints provided by the central PO segments that are covalently bonded to the EO blocks. The driving force for the formation of the inclusion crystals derives from the mutual interaction of aromatic units along the channels with target copolymer chains. This driving force, the CH···π intermolecular interactions, endows the network with robustness and high thermal stability. The chemical linkages between the EO and PO sequences in block copolymers force the EO units, which are aligned in the crystalline lamellae, to be tethered to next parallel lamellae, while the PO segments reside at the interface of the two rigid crystallites. Notably, the thickness of the inclusion compound crystallites can be tuned by the length of the end EO blocks, providing access to a broad range of domain sizes and offering intriguing perspectives to modulate the sizes of alternated crystalline and amorphous domains.

Bulk preparation of the compounds can be achieved by direct mechanochemical assembly of the host and the copolymer mixture. The facile self-assembly of two components was followed in situ by synchrotron powder X-ray diffraction, straightforwardly demonstrating the formation of the hexagonal phase of

the inclusion compound by the thermal treatment. A more complete description of the structure could be achieved by fast-^{1}H MAS and 2D ^{1}H−^{13}C heterocorrelated NMR techniques that could discriminate the copolymer sequences in the distinct environments, the amorphous and supramolecular crystalline domains, and identify noncovalent intermolecular interactions. The nanochannels in the inclusion crystals are lined with aromatic groups that produce a large upfield shift on the NMR signals of the guests due to the magnetic susceptibility. The relationship of magnetic subsceptibility effect versus host−guest internuclear distances could be understood by HF-GIAO/DGDZVP theoretical calculations, supporting the existence of intermolecular CH$\cdots\pi$ interactions and enforcing the model of high specificity in the incorporation of selected blocks in the nanocrystals.

The potential of creating a diversity of nanoscopic structures based on block copolymers can be further enriched by the present strategy involving the use of inclusion crystal self-assembly. Such a strategy provides control over the supramolecular organization and can greatly modulate the intermolecular interactions; therefore, we can expect this approach to be used for the design of novel functional materials with various applications, including the fabrication of photonic crystals.

EXPERIMENTAL SECTION

Preparation of TPP and Inclusion Compounds. Poly(ethylene oxide-*co*-propylene oxide) copolymers denominated F68, F108, and random copolymer were purchased from Sigma-Aldrich, while poly(ethylene oxide-*co*-propylene oxide) copolymers denominated PE6800 and F127 were purchased from BASF. The microstructures of the copolymers were determined by ^{1}H NMR spectroscopy. The synthesis of TPP was carried out starting from a solution of 10.8 g of *o*-phenylenedioxy in 27.5 mL of triethylamine and 90 mL of anhydrous THF that was added dropwise under stirring and refluxing to sublimated hexachlorophosphazene (11.53 g) dissolved in 175 mL of THF. The triethylamine was first dried over calcium hydride for 1 h and then filtered. Stirring and refluxing was continued for 40 h at 60 °C. The white precipitate was filtered off, and washed with THF and then distilled water (3 L). Extraction with benzene in a Kumagawa apparatus, and then crystallization in benzene, yielded the TPP/benzene IC. The guest-free TPP crystalline structure in the hexagonal form was obtained by thermal treatment of TPP/benzene IC at 75 °C under vacuum for 1 h, while the thermal treatment of TPP/benzene IC at 185 °C under vacuum for 6 h generates the close-packed monoclinic structure. The stoichiometries of the resulting inclusion compounds were confirmed by ^{1}H NMR spectroscopy. ^{1}H NMR spectra were recorded on a Varian 400 MHz Mercury spectrometer. The inclusion compounds with both the block copolymers and the random copolymers were crystallized from *o*-xylene solutions containing the dissolved TPP and the corresponding guest. The formation of the TPP/copolymer adducts could be obtained by grinding of the TPP and copolymer mixture at room temperature or by melting the TPP and copolymer mixture at 343 K. No inclusion compound with pure poly(propylene oxide) homopolymer was formed.

Synchrotron X-ray Diffraction. In-situ synchrotron X-ray powder diffraction experiments were performed at the European Synchrotron Radiation Facility (ESRF) in Grenoble on the BeamLine Gilda-BM08, with a Debye−Scherrer type diffractometer equipped with a gas handling system.[34] The radiation wavelength λ of the incident X-rays was 0.78 Å; the 2θ range was from 2° to 40°. The powder samples were loaded into a glass capillary, inner diameter 0.8 mm. The powder X-ray diffraction patterns were performed at variable temperature, from room temperature to 630 K at different heating rates ranging from 0.5 to 1 K/min. The Rietveld refinements of the crystal structures at each temperature were performed by the GSAS computer package.[35] A Chebyshev polynomial of first kind with 12 coefficients was used to model the intensity background, and the peak shape was represented by a convolution of a pseudo-Voigt function.

Solid-State NMR. ^{1}H Fast-MAS NMR spectra were collected at 500 MHz on a Bruker Avance 500 instrument equipped with a 2.5 mm double resonance MAS probe. The samples were spun at the magic angle at a spinning speed of 35 kHz NMR, and a recycle delay of 10 s was applied. The 90° pulse for proton was 2.9 μs. The ^{13}C solid-state NMR spectra were run at 75.5 MHz on a Bruker Avance 300 instrument operating at a static field of 7.04 T equipped with 4 mm double resonance MAS probe. The samples were spun at the magic angle at a spinning speed of 15 kHz, and ramped-amplitude cross-polarization (RAMP-CP) transfer of magnetization was applied. The 90° pulse for proton was 2.9 μs. ^{13}C Single-pulse excitation (SPE) experiments were run using a recycle delay of 5 s, and cross-polarization (CP) MAS experiments were performed using a recycle delay of 10 s and contact times of 0.5 and 2.5 ms. Phase-modulated Lee−Goldburg (PMLG) heteronuclear ^{1}H−^{13}C correlation (HETCOR) experiments coupled with fast magic angle spinning (15 kHz) allowed the recording of 2D spectra with high resolution both in the hydrogen and in the carbon dimensions. Narrow hydrogen resonances, with line widths in the order of 1−2 ppm, were obtained with homonuclear decoupling during t_1; this resolution permits a sufficiently accurate determination of the proton species present in the system. PMLG ^{1}H−^{13}C HETCOR spectra were run with LG period of 18.9 μs. The efficient transfer of magnetization to the carbon nuclei was performed applying RAMP-CP sequence. Quadrature detection in t_1 was achieved by time proportional phase increments method. Carbon signals were acquired during t_2 under proton decoupling applying the two-pulse phase modulation scheme (TPPM).

Computational Study. Quantum-chemical calculations were performed with the Gaussian 03 package. Proton shielding was calculated using the GIAO method at the HF level and employing DGDZVP basis set. The proton chemical shifts were given relative to the tetramethylsilane (TMS) calculated at the GIAO-HF/DGDZVP level. The geometries of the phenylenedioxyphosphate and the methane molecules were optimized at the B3LYP/6-311G(d,p) level. The phenylenedioxyphosphate aromatic molecule is planar, and its Cartesian coordinates were oriented in the *XY* plane. Methane molecule with the C−H bond aligned perpendicular to the aromatic plane was placed at distinct *Z* distances of 2.5, 2.75, 2.85, 3, 3.25, 3.5, 4, 4.5, and 5 Å above the phenylenedioxyphosphate, and at each *Z* level a grid that extended along the *X,Y* axis was explored. Single point NMR calculations were performed for each position. The isotropic shielding value beside the aromatic ring was calculated placing the C−H methane bond parallel to the aromatic plane and moving the CH_4 with 0.5 Å increments in the *X*, *Y*, and *Z* directions in separate calculations. The shielding increments $\Delta\sigma = \sigma_{CH4\text{-}Phen} - \sigma_{CH4\text{-}free}$ were calculated as the difference between the isotropic shielding value of the methane hydrogen at a given point in the Cartesian space and that of the isolated methane. The chemical shift changes $\Delta\delta = \delta_{CH4\text{-}Phen} - \delta_{CH4\text{-}free}$ are equal in magnitude but opposite in sign to the shielding increments ($\Delta\sigma = -\Delta\delta$).

Scanning Electron Microscopy. SEM was performed on a Tescan Mira3 field emission scanning electron microscope operating at 5 kV. The samples were coated with a thin layer of gold before imaging.

ASSOCIATED CONTENT

Supporting Information. DSC thermograms of the adducts, synchrotron powder X-ray diffraction patterns of the host matrix as a function of temperature, Rietveld refinement of the synchrotron X-ray diffraction patterns of the adducts, and ^{1}H NMR spectra in solution of pure copolymers and their adducts.

This material is available free of charge via the Internet at http://pubs.acs.org.

AUTHOR INFORMATION

Corresponding Author
angiolina.comotti@mater.unimib.it

ACKNOWLEDGMENT

This study was partially supported by Fondazione Cariplo and FIRB (Ministry of Education and Research). We thank Dr. Z. Kral and Dr. G. Casati from TESCAN for technical support in collecting SEM images. G. Distefano is acknowledged for his contribution in the synthesis and B. Moltrasio for his contribution to computational calculations. S.B. is grateful for financial support from the FIRB Research Fellowship for Young Scientists.

REFERENCES

(1) (a) Lehn, J.-M. *Science* **2002**, *295*, 2400.

(2) (a) Bates, F. S.; Fredrickson, G. H. *Phys. Today* **1999**, *52*, 32. (b) Binder, K. *Adv. Polym. Sci.* **1994**, *112*, 181. (c) Stupp, S. I. *Curr. Opin. Colloid Interface Sci.* **1998**, *3*, 20. (d) Bates, F. S.; Fredrickson, G. H. *Annu. Rev. Phys. Chem.* **1990**, *41*, 525.(e) Hamley, I. W. *The Physics of Block Copolymers*; Oxford University Press: Oxford, 1998.

(3) (a) Cornelissen, J. J. L. M.; Fischer, M.; Sommerijk, N. A. J. M.; Nolte, R. J. M. *Science* **1998**, *280*, 1427. (b) Kang, Y.; Walish, J. J.; Gorishnyy, T.; Thomas, E. L. *Nat. Mater.* **2007**, *6*, 957.

(4) (a) Jain, S.; Bates, F. S. *Science* **2003**, *300*, 460. (b) Thurn-Albrecht, T.; Schotter, J.; Kastle, G. A.; Emley, N.; Shibauchi, T.; Krusin-Elbaum, L.; Guarini, K.; Black, C. T.; Tuominen, M. T.; Russell, T. P. *Science* **2000**, *290*, 2126. (c) Jenekhe, S. A.; Chen, X. L. *Science* **1998**, *279*, 1903. (d) Shefelbine, T. A.; Vigild, M. E.; Cussler, E. L.; Bates, F. S.; Matsen, M. W.; Hajduk, D. A.; Hillmyer, M. A. *J. Am. Chem. Soc.* **1999**, *121*, 8457. (e) Lee, S.; Bluemle, M. J.; Bates, F. S. *Science* **2010**, *330*, 349.

(5) (a) Zhao, D. Y.; Feng, J. L.; Huo, Q. S.; Melosh, N.; Fredrickson, G. H.; Chemlka, B. F.; Stucky, G. D. *Science* **1998**, *279*, 548. (b) Warren, S. C.; Messina, L. C.; Slaughter, L. S.; Kamperman, M.; Zhou, Q.; Gruner, S. M.; DiSalvo, F. J.; Wiesner, U. *Science* **2008**, *320*, 1748. (c) Tian, B.; Liu, X.; Solovyov, L. A.; Liu, Z.; Yang, H.; Zhang, Z.; Xie, S.; Zhang, F.; Tu, B.; Yu, C.; Terasaki, O.; Zhao, D. *J. Am. Chem. Soc.* **2004**, *126*, 865. (d) Lee, M.; Park, M.-H.; Oh, N.-K.; Zin, W.-C.; Jung, H.-T.; Yoon, D. K. *Angew. Chem., Int. Ed.* **2004**, *43*, 6466. (e) Pai, R. A.; Humayun, R.; Schulberg, M. T.; Sengupta, A.; Sun, J. N.; Watkins, J. J. *Science* **2004**, *303*, 507. (f) Templin, M.; Franck, A.; DuChesne, A.; Leist, H.; Zhang, Y. M.; Ulrich, R.; Schadler, V.; Wiesner, U. *Science* **1997**, *278*, 1795.

(6) (a) Zalusky, A. S.; Olayo-Valles, R.; Wolf, J. H.; Hillmyer, M. A. *J. Am. Chem. Soc.* **2002**, *124*, 12761. (b) Koo, C. M.; Wu, L.; Lim, L. S.; Mahanthappa, M. K.; Hillmyer, M. A.; Bates, F. S. *Macromolecules* **2005**, *38*, 6090. (c) Mao, H.; Hillmyer, M. A. *Soft Matter* **2006**, *2*, 57. (d) Thomas, E. L.; Anderson, D. M.; Henkee, C. S.; Hoffman, D. *Nature* **1988**, *334*, 598. (e) Ruokolainen, J.; Makinen, R.; Torkkeli, M.; Makela, T.; Serimaa, R.; Brinke, G. T.; Ikkala, O. *Science* **1998**, *280*, 557.

(7) Chen, Z.-R.; Kornfield, J. A.; Smith, S. D.; Grothaus, J. T.; Satkowski, M. M. *Science* **1997**, *277*, 1248.

(8) (a) Lee, M.; Cho, B.-K.; Zin, W.-C. *Chem. Rev.* **2001**, *101*, 3869. (b) Webster, O. W. *Science* **1991**, *251*, 887. (c) Hadjichristidis, N.; Pitsikalis, M.; Pispas, S.; Iatrou, H. *Chem. Rev.* **2001**, *101*, 3747. (d) Deming, T. J. *Nature* **1997**, *390*, 386.

(9) (a) Balazs, A. C.; Emrick, T.; Russell, T. P. *Science* **2006**, *314*, 1107. (b) Lin, Y.; Boker, A.; He, J.; Sill, K.; Xiang, H.; Abetz, C.; Li, X.; Wang, J.; Emrick, T.; Long, S.; Wang, Q.; Balazs, A. C.; Russell, T. P. *Nature* **2005**, *434*, 55. (c) Hamley, I. W. *Angew. Chem., Int. Ed.* **2003**, *42*, 1692.

(10) (a) Hajduk, D. A.; Harper, P. E.; Gruner, S. M.; Honeker, C. C.; Kim, G.; Thomas, E. L.; Fetters, L. J. *Macromolecules* **1994**, *27*, 4063. (b) Valkama, S.; Kosonen, H.; Ruokolainen, J.; Haatainen, T.; Torkkeli, M.; Serimaa, R.; Ten Brinke, G.; Ikkala, O. *Nat. Mater.* **2004**, *3*, 872. (c) Tirumala, V. R.; Romang, A.; Agarwal, S.; Lin, E. K.; Watkins, J. J. *Adv. Mater.* **2008**, *20*, 1603.

(11) (a) Li, J.; Ni, X.; Zhou, Z.; Leong, K. W. *J. Am. Chem. Soc.* **2003**, *125*, 1788. (b) Hsin-Fang Lee, H.-F.; Sheu, H.-S.; Jeng, U. S.; Huang, C. F.; Chang, F. C. *Macromolecules* **2005**, *38*, 6551.

(12) (a) Miyata, M.; Tohnai, N.; Hisaki, I. *Acc. Chem. Res.* **2007**, *40*, 694.(b) Miyata, M.; Sada, K. *Comprehensive Supramolecular Chemistry, Solid-state Supramolecular Chemistry: Crystal Engineering*; Pergamon: Oxford, 1996; Vol. 6, pp 147−176.

(13) (a) Toudic, B.; Garcia, P.; Odin, C.; Rabiller, P.; Ecolivet, C.; Collet, E.; Bourges, P.; McIntyre, G. J.; Hollingsworth, M.; Breczewski, T. *Science* **2008**, *319*, 5859. (b) Harris, K. D. M. *Chem. Soc. Rev.* **1997**, *26*, 279.

(14) (a) Farina, M.; Di Silvestro, G.; Sozzani, P. *Comprehensive Supramolecular Chemistry, Solid-state Supramolecular Chemistry: Crystal Engineering*; Pergamon: Oxford, UK, 1996; Vol. 6, pp 371−419. (b) Schilling, F. C.; Amundson, K. R.; Sozzani, P. *Macromolecules* **1994**, *27*, 6498. (c) Sozzani, P.; Bovey, F. A.; Schilling, F. C. *Macromolecules* **1991**, *24*, 6764. (d) Sozzani, P.; Bovey, F. A.; Schilling, F. C. *Macromolecules* **1989**, *22*, 4225.

(15) (a) Sozzani, P.; Bracco, S.; Comotti, S.; Simonutti, R. *Adv. Polym. Sci.* **2005**, *181*, 153. (b) Sozzani, P.; Comotti, A.; Bracco, S.; Simonutti, R. *Chem. Commun.* **2004**, 768. (c) Allcock, H. R.; Primrose, A. P.; Sunderland, N. J.; Rheingold, A. L.; Guzei, I. A.; Parvez, M. *Chem. Mater.* **1999**, *11*, 1243. (d) Comotti, A.; Simonutti, R.; Catel, G.; Sozzani, P. *Chem. Mater.* **1999**, *11*, 1476.

(16) (a) Sozzani, P.; Comotti, A.; Bracco, S.; Simonutti, R. *Angew. Chem., Int. Ed.* **2004**, *43*, 2811. (b) Sozzani, P.; Bracco, S.; Comotti, A.; Ferretti, L.; Simonutti, R. *Angew. Chem., Int. Ed.* **2005**, *44*, 1816. (c) Brustolon, M.; Barbon, A.; Bortolus, M.; Maniero, A. L.; Sozzani, P.; Comotti, A.; Simonutti, R. *J. Am. Chem. Soc.* **2004**, *126*, 15512.

(17) Bracco, S.; Comotti, A.; Beretta, M.; Valsesia, P.; Sozzani, P. *Cryst. Eng. Commun.* **2010**, *12*, 2318.

(18) (a) Tanaka, K.; Toda, F. *Chem. Rev.* **2000**, *100*, 1025. (b) Trask, A. V.; Jones, W. *Top. Curr. Chem.* **2005**, *254*, 41. (c) Nguyen, K. L.; Friscic, T.; Day, G. M.; Gladden, L. F.; Jones., W. *Nat. Mater.* **2007**, *6*, 206. (d) Shan, N.; Jones, W. *Green Chem.* **2003**, *5*, 728. (e) Sokolov, A.; Swenson, D. C.; MacGillivray, L. R. *Proc. Natl. Acad. Sci. U.S.A.* **2008**, *105*, 1794. (f) Etter, M. C.; Reutzel, S. M.; Choo, C. G. *J. Am. Chem. Soc.* **1993**, *115*, 4411.

(19) (a) Sozzani, P.; Comotti, A.; Simonutti, R.; Meersmann, T.; Logan, J. W.; Pines, A. *Angew. Chem., Int. Ed.* **2000**, *39*, 2695. (b) Meersmann, T.; Logan, J. W.; Simonutti, R.; Caldarelli, S.; Comotti, A.; Sozzani, P.; Kaiser, L. G.; Pines, A. *J. Phys. Chem. A* **2000**, *104*, 11665. (c) Comotti, A.; Bracco, S.; Ferretti, L.; Mauri, M.; Simonutti, R.; Sozzani, P. *Chem. Commun.* **2007**, 350.

(20) (a) Comotti, A.; Simonutti, R.; Stramare, S.; Sozzani, P. *Nanotechnology* **1999**, *10*, 70. (b) Allcock, H. R.; Levin, M. L.; Whittle, R. R. *Inorg. Chem.* **1986**, *25*, 41.

(21) For comparison purposes, powder X-ray diffraction patterns were collected as a function of temperature of the porous pure TPP hexagonal phase in the absence of the copolymer. At 373−423 K, the hexagonal phase of the empty TPP transforms into the more stable close-packed structure.

(22) Bovey, F. A.; Mirau, P. *NMR of Polymers*; Academic Press: San Diego, CA, 1996.

(23) (a) van Rossum, B.-J.; de Groot, C. P.; Ladizhansky, V.; Vega, S.; de Groot, H. J. *J. Am. Chem. Soc.* **2000**, *122*, 3465. (b) Sozzani, P.; Bracco, S.; Comotti, A.; Simonutti, R.; Camurati, I. *J. Am. Chem. Soc.* **2003**, *125*, 12881.

(24) (a) Waugh, S.; Fessenden, R. W. *J. Am. Chem. Soc.* **1957**, *79*, 846. (b) Johnson, C. E.; Bovey, F. A. *J. Chem. Phys.* **1958**, *29*, 1012. (c) Von RaguéSchleyer, P.; Maerker, C.; Dransfeld, A.; Jiao, H.; Van Eikema Hommes, N. J. R. *J. Am. Chem. Soc.* **1996**, *118*, 6317. (d) Canceill, J.; Lacombe, L.; Collet, A. *J. Am. Chem. Soc.* **1986**, *108*, 4230. (e) Rapp, A.; Schnell, I.; Sebastiani, D.; Brown, S. P.; Percec, V.; Spiess, H. W. *J. Am. Chem. Soc.* **2003**, *125*, 13284.

(25) The linewidth of the crystalline phase component is attributed to motional broadening: Schantz, S. *Macromolecules* **1997**, *30*, 1419.

(26) In the crystalline phase of bulk poly(ethylene oxide), the dihedral angle on $-CH_2-O-$, which is effective on the chemical shift, is 180°, and the CH_2 carbons do not experience any γ-gauche effect: (a) Takahashi, Y.; Tadokoro, H. *Macromolecules* **1973**, *6*, 672. (b) Tonelli, A. *Macromolecules* **1978**, *11*, 565.

(27) Farina, M.; Natta, G.; Allegra, G.; Loffelholz, M. *J. Polym. Sci., Part C* **1967**, *16*, 2517.

(28) (a) Vinogradov, E.; Madhu, P. K.; Vega, S. *Chem. Phys. Lett.* **1999**, *314*, 443. (b) Vega, S. *Chem. Phys. Lett.* **2007**, *447*, 370. (c) Uemura, T.; Horike, S.; Kitagawa, K.; Mizuno, M.; Endo, K.; Bracco, S.; Comotti, A.; Sozzani, P.; Nagaoka, M.; Kitagawa, S. *J. Am. Chem. Soc.* **2008**, *130*, 6781. (d) Sozzani, P.; Bracco, S.; Comotti, A.; Mauri, M.; Simonutti, R.; Valsesia, P. *Chem. Commun.* **2006**, 1921. (e) Comotti, A.; Bracco, S.; Sozzani, P.; Hawxwell, S. M.; Hu, C.; Ward, M. D. *Cryst. Growth Des.* **2009**, *9*, 3000.

(29) The low multiplicity of the TPP signals indicates the high symmetry of the TPP molecule in the hexagonal honeycomb structure in agreement with the X-ray diffraction structure.

(30) Frisch, M. J.; et al. *Gaussian 03*, revision C.02; Gaussian, Inc.: Wallingford, CT, 2004.

(31) The methane molecule was set with the C−H bond perpendicular to the aromatic plane in the shielding cone and at the magic angle, and parallel in the deshielding cone.

(32) Takahashi, O.; Kohno, Y.; Nishio, M. *Chem. Rev.* **2010**, *110*, 6049.

(33) ^{1}H solid-state NMR spectrum of TPP/F108 adduct indicates that a 0.8 molar fraction of EO (EO_{in}/EO_{tot}) is included in the host matrix that corresponds to about 100 EO_{in} monomer units over 132 (each EO segment consists of 132 mu). Considering that the portion of the nanochannel occupied by a monomer unit is 3.5 Å, the overall height of a single crystalline lamella is 35 nm. The height of the amorphous phase was estimated considering that 52 PO units plus 2 times 32 EO_{out} units participate in the amorphous phase, a single chain protruding out of the crystalline lamella insists on an area of 2 nm^2 (the area of 2 nm^2 on the $a-b$ plane was calculated as 1.004^2 $nm^2 \times \cos 30° \times 2$), and the density amorphous phase is about 1 g/cm^3.

(34) Meneghini, B.; Artioli, G.; Balerna, A.; Gualtieri, A. F.; Norby, P.; Mobilio, S. *J. Synchrotron Radiat.* **2001**, *8*, 1162.

(35) (a) Larson, A. C.; Von Dreele, R. B. *GSAS: Generalized Structure Analysis System Manual*; Los Alamos National Laboratory Report LAUR-86-748; U.S. Government Printing Office: Washington, DC, 1994. (b) Von Dreele, R. B.; Jorgensen, J. D.; Windsor, C. G. *J. Appl. Crystallogr.* **1982**, *15*, 581.